RSC Advances

ROYAL SOCIETY OF CHEMISTRY

www.rsc.org/advances

RSC Advances

ARTICLE

Prediction of particle deposition and layer growth in preparation of a dynamic membrane with cross-flow microfiltration

Received 00th January 20xx,
Accepted 00th January 20xx

DOI: 10.1039/x0xx00000x

www.rsc.org/

Yanqiu Pan,[a] Wenjuan Wang,[a] Wei Wang[b]* and Tonghua Wang[a]

Theoretical and experimental investigations were conducted to predict particle deposition and layer growth during formation of a dynamic membrane using cross-flow microfiltration. Critical particle size model was developed and solved in radial, circumferential and axial directions by analyzing the forces acting on a single particle. The models accounted for the normal drag, lateral lift, shear-induced and Brownian diffusion forces in the depositional direction, the Van der Waals force in the circumferential direction, and the cross-flow drag and Van der Waals forces in the axial direction. Cross-flow velocity and feed temperature were selected as representative influencing factors to examine variations of the critical particle sizes with permeate flux. Experiments were then conducted with carbon tubes as the support and zirconium dioxide particles as the coating material to verify the model. Results showed that a dynamic layer with non-uniform thickness along the circumferential direction was formed within the horizontal tube due to gravity. The layer thickness decreased as the cross-flow velocities were increased under given trans-membrane pressure difference and feed concentration. An appropriately large cross-flow velocity was beneficial to achieve thickness uniformity during formation. The effect of the feed temperature on the critical particle size and layer thickness can be ignored. Comparisons between the theoretical predictions and experimental data of the layer thicknesses displayed good agreements. The effects of trans-membrane pressure differences and feed concentrations were finally examined in the present work.

Introduction

Dynamic membrane (DM) is a type of hysteromorphous membranes that are formed on the surface of porous supports, such as ceramic, carbon and polymeric membranes. Because particles in liquids are similar in size to the support pores, they are rejected and deposited onto the support surface, forming a dynamic layer. Both the dynamic layer and the support constitute an asymmetrical structure, and its overall rejection performances are superior to the support.[1–3] DM has the properties of ultrafiltration and/or microfiltration membranes, which is characterized by easy preparation, operation and cleaning. According to its formation modes, DM can be classified into two types, self-formed and pre-coated DMs. The former is a cake layer formed on supports by particles in feed liquids to be separated, and the latter is a pre-coated cake layer with a type of pre-designated particle before filtration. The self-formed DM is easily operated and washed but challenging to maintain a stable performance. The pre-coated type can have an improved performance controllable through surface modification of the support to form a hybrid DM, which has recently become a hot topic in research and development.

Due to its brilliant anti-fouling ability, DMs are quite suitable for protein recovery[4,5] as well as domestic and industrial wastewater treatment.[6–8] Previous experimental investigations of DMs have mainly concentrated on examining the effects of operating conditions, such as cross-flow velocities, feed flow rates, trans-membrane pressure differences and feed concentrations on permeation. Special attentions have been paid to the permeate flux and rejection rate. Fluxes that are larger than or at least the same as those of ordinary membranes have been achieved,[9–11] and over 98% of rejection rates have been attained,[4,8,12] which all meet process requirements. In terms of modeling research, membrane fouling-related mechanisms are quite helpful for understanding the DM formation process because DMs were in fact derived from membrane fouling.[13] Through comparing mean geometric sizes between membrane-forming particles and support pores, Tanny summarized four DM classes, i.e., complete blocking filtration, intermediate blocking filtration, standard blocking filtration and cake layer filtration.[14] In preparing a MnO_2 DM on top of a polyester primary membrane, AlMalack and Anderson reported that the dynamic layer was formed according to standard blocking filtration when the particle sizes were smaller than those of the primary membrane, and later cake filtration was achieved as particles started to bridge the pores and precipitate onto the membrane surface.[15] Vincent-Vela *et al*. found that the

[a] State Key Laboratory of Fine Chemicals, School of Chemical Engineering, Dalian University of Technology, Dalian, China.
[b] State Key Laboratory of Fine Chemicals, School of Chemical Machinery and Safety, Dalian University of Technology, Dalian, China.
* E-mail: dwwang@dlut.edu.cn or yqpan@dlut.edu.cn; Fax: +86 411 84986020; Tel: +86 411 84986020

controlling factor of fouling was intermediate blocking filtration under high fouling conditions in experimental discussion of fouling resistances during DM filtration.[16] However, this type of model is actually a phenomenological one that can be used only to analyze and fit the experimental data but cannot predict flux quantity. Therefore, this model cannot be called a realistic mechanism model.

Since the 1970s, substantial efforts have been devoted to the mathematical modeling of flux prediction in the DM process based on different mechanisms. The representative models are the shear-stress diffusion model, concentration polarization model and force balance model. For the first one, Pillay considered three obvious mass transfer phenomena on the dynamic layer, i.e., radial flow induced conduction of the particles towards the membrane surface and shear-stress induced diffusions of particles from the dynamic layer to the boundary layer and from the boundary layer to the bulk stream.[17] Such diffusions are caused not only by Brownian diffusion but also by interactions between fluids and particles. Davis and Leighton, Romero and Davis, Song, Wang and Song developed their separate shear-stress diffusion models by accounting for the tangential speed distribution of the fluid and dividing the membrane into equilibrium and non-equilibrium regions along the axial direction.[18–21] The concentration polarization model was based on the concentration difference that was as the driving force of mass transport between the bulk stream and the dynamic layer with the boundary layer close to the laminar flow. Schulz and Ripperger, Hunt *et al.* and Perkins *et al.* developed their own similar models.[22–24] Before the permeate flux had been stabilized, the particle concentration, fluid velocity and pressure varied along the radial direction; when the flux was stabilized, the particle quantity transported from the bulk stream to the membrane surface was equal to the quantity from the membrane surface back to the bulk stream. Based on classical mechanics, Blake *et al.* proposed a force balance model by analyzing the forces exerting on a single particle deposited on the dynamic layer.[25] Only the axial forces, including the drag force caused by the radial flow, frictional force and molecular force between the particles were considered in the development of the steady-state flux model for cross-flow filtration. Altmann and Ripperger introduced hydrodynamic, adhesive and frictional forces acting on a single particle into their model of layer formation and cake growth during cross-flow microfiltration and obtained a good correlation between the model calculations and the experimental results at a constant trans-membrane pressure.[26] Chang *et al.* developed a similar mathematical model based on moment balance of the hydrodynamic and inter-particle forces acting on a single spherical particle and showed satisfactory prediction results with experimental measurements of the quasi-steady-state permeate flux.[27]

In general, attributes of a desired pre-coated DM should be complete and uniform coverage of coating particles on substrate, and controllable layer thickness with a small and/or an acceptable resistance. Although efforts have been made to model DM phenomena, only a few publications have predicted particle deposition and layer growth during DM formation. The shear-stress diffusion model and the concentration polarization model can simply be used to predict permeate flux variations, and the available force balance model only accounted for the unidirectional forces acting on the particles. Prediction of particle deposition and layer growth during DM formation is far from perfect. A comprehensive model that considers multi-directional forces still remains necessary. The objectives of the present study were to first develop critical particle size model in radial, circumferential and axial directions to simulate three critical particle sizes and DM thickness, and then to conduct DM preparation experiments to verify the model with porous carbon tube as the support and zirconium dioxide (ZrO_2) particles as the coating material, and finally to predict particle deposition and layer growth under various operating conditions. This fundamental research is expected to provide a helpful tool for future design, operation and control of the DM process.

Mathematical model

Cross-flow microfiltration is a complex process that can be affected by many factors, including cross-flow velocity, feed temperature, trans-membrane pressure difference and feed concentration, as well as support and coating material properties. Since DM formation is similar to cake formation in cross-flow filtration, the developed mathematical model was based on the force balance principle of a particle in an attempt to predict the critical particle sizes and layer thickness during preparation. The main assumptions made in the model formulation were as follows: rigid particles, incompressible fluid, instantaneous complete particle deposition without re-suspension and laminar flow of fluids within the pores of both the dynamic layer and support.

Critical particle size of radial deposition

Figure 1 shows the forces acting on a single particle. Due to bilateral symmetry, a particle located on the left side of the circumference was chosen for force analysis, and the intersection angle, ϕ, was the angle between the gravitational and depositional directions. As seen in Fig. 1(b), five forces were exerted on the particle in the radial direction. These forces were the component, $F_w\cos\phi$, of the gravity, F_w, and the other four forces, i.e., the normal dray force, F_y, due to permeation flow, the lateral lift force, F_a, due to cross-flow, the shear-induced force, F_b, and the Brownian diffusion force, F_c. The resultant force of the four forces in the radial direction is denoted as F_A in Figs. 1(c) and 1(d).

Due to the laminar flow, the normal drag force, F_y, was estimated using the Stokes equation,[26] as follows:

$$F_y = 3\pi\mu d_p J(t) \quad (1)$$

where μ (Pa s) is the fluid viscosity of feed, d_p (m) is the particle diameter and J (m^3 m^{-2} s^{-1}) is the permeate flux. According to theoretical and experimental investigations, the lateral lift force, F_a, was calculated below.[26]

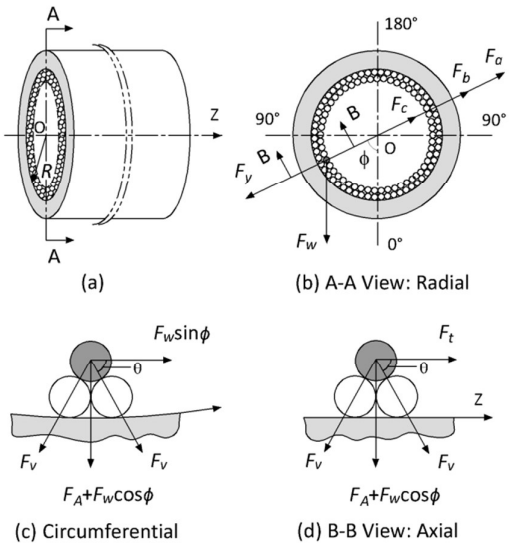

Fig. 1 Forces acting on a single particle. (a) A section of cylindrical DM; (b) A-A view: radial force analysis; (c) circumferential force analysis; (d) B-B view: axial force analysis.

$$F_a = \frac{0.761\tau_w^{1.5} d_p^3 \rho^{0.5}}{\mu} \quad (2)$$

where ρ (kg m^{-3}) is the feed fluid density and the surface shear-stress, τ_w (N m^{-2}), can be found in the literature.[28]

$$\tau_w = 0.0233\left(\frac{\mu}{R}\right)^{0.25}\rho^{0.75}U^{1.75}$$

where R (m) is the inner radius of the tubular support and U (m s^{-1}) is the cross-flow velocity.

Because the diameter of coating particles used in subsequent experiments was less than 20 μm, the shear-induced force, F_b, and the Brownian diffusion force, F_c, were taken into account.[29] It was known that particle quantity transported from bulk fluid to the dynamic layer surface would equal the quantity from the surface back to bulk fluid when the steady permeate flux was achieved.[22–24] In an addition to the lateral migration, the shear-induced and Brownian diffusions were the two major mechanisms to govern this back transport, which were all in the opposite depositional direction.[29–31] Brownian diffusion favored the transport of smaller particles while the shear-induced diffusion increased as particle sizes increased.[29] The F_b and F_c were obtained by the following equations:[27,29,31]

$$F_b = \frac{3\pi\mu d_p^3 U}{20R^2} \quad (3)$$

$$F_c = \frac{kT}{R} \quad (4)$$

where k (J K^{-1}) is the Boltzmann constant and T (K) is the feed temperature.

The resultant force, F_A, of the four forces in the radial direction, as shown in Fig. 1(b), is written below.

$$F_A = F_y - F_a - F_b - F_c$$

The net gravity of a particle is the difference between its own gravity and buoyancy, as follows:

$$F_w = \frac{\pi}{6}(\rho_s - \rho)d_p^3 g \quad (5)$$

where ρ_s (kg m^{-3}) is the particle density.

During DM formation on the inner surface of a horizontal tubular support, the particles at different locations along the circumferential direction would experience different resultant forces in the radial direction. The resultant force of the five forces can therefore be written as follows:

$$F = F_A + F_W\cos\phi \quad (6)$$

When the resultant force, F, was above zero, as shown in Fig. 1(b), the particle was deposited; otherwise, it was not deposited. When the F was zero, the corresponding particle diameter determined the maximum possible diameter for particle deposition in the radial direction, which was called the critical particle size of radial deposition, $d_{crit,R}$.

Critical particle size of circumferential rolling

Due to the gravitational effect, the particles deposited on the inner surface of support may roll along the circumferential direction, which would affect the DM uniformity. In addition to the radial resultant force, Hamaker proposed that the Van der Waals force should be considered,[32] as shown in Fig. 1(c).

$$F_v = \frac{-Ad_p^2}{12H(H+d_p)}\left[\frac{-\left(4H^2+3d_pH+d_p^2\right)}{H(H+d_p)^2}+\frac{4}{H+2d_p}\right] \quad (7)$$

where A (J) is a constant, which equals 10^{-6} based on Hamaker's recommended value,[32] and H (m) represents the shortest distance between two neighboring particles.[33]

$$H = \left[\left(\frac{\pi}{K\left[1-\varepsilon(t)\right]}\right)^{0.33}-1\right]d_p$$

where $\varepsilon(t)$ is the porosity of the dynamic layer and K is a parameter related to the packing structure, which was calculated using the following formula by assuming that the deposited particles were hexagonally arrayed:

$$K = 3\cos(90-\theta)$$

where θ was 54.7° for hexagonal packing.[34] It should be pointed out that introduction to the K has considered interactions between a surface particle and all of the three neighbors below it. The inter-particle forces on the layer surface would be zero because of the symmetrical packing structure. Resultant force of the Van der Waals forces was oriented to the depositional direction.

Through force analysis in Fig. 1(c), the moment balance equation in the circumferential direction can be written as follows:

$$M_C = \frac{d_p}{2}\left[(F_A + F_w\cos\phi + KF_v)\cos\theta - F_w\sin\phi\sin\theta\right] \quad (8)$$

When the moment, M_C, was below zero, the particle would roll along the circumferential direction; otherwise, it would not

roll. When the M_C equaled zero, the particle was in a critical state, and the corresponding particle diameter was called the critical particle size of circumferential rolling, $d_{crit,C}$.

Critical particle size of axial rolling

Due to cross-flow, a drag force along the axial direction exists. The deposited particles may roll on the inner support surface along the axial direction. The drag force has been considered to be 2.11 times the value of the Stokes force.[26]

$$F_t = 3.16\pi\tau_w d_p^{\,2} \tag{9}$$

Therefore, a similar force analysis in Fig. 1(d) can be utilized to obtain the moment balance equation in the axial direction, as follows:

$$M_R = \frac{d_p}{2}[(F_A + F_w\cos\phi + KF_v)\cos\theta - F_t\sin\theta] \tag{10}$$

When the M_R equaled zero, the corresponding particle diameter is called the critical particle size of axial rolling, $d_{crit,A}$.

Thickness of dynamic layer

When preparing a DM, pore blockage and cake formation are two essential processes to consider. In dead-end microfiltration, all particles that reach the substrate surface would eventually deposit onto the surface. In cross-flow microfiltration, however, only a fraction of the particles can deposit onto the surface at each circle.[20] After the pore blockage stage, a circle of cake growth begins until the DM thickness remains stable. By modifying the particle deposition rate equation, Altmann and Ripperger determined the mass growth rate equation,[26] as follows:

$$m(t) = J(t)\frac{\rho_s c_s}{\rho_s - c_s}Q_m(d_{crit}) \tag{11}$$

where c_s (kg m^{-3}) is the particle mass concentration within the feed. The mass growth rate, $m(t)$ (kg m^{-2} s^{-1}), is related not only to the permeate flux but also to the mass accumulation fraction, Q_m. The mass accumulation fraction of the particles depended on the critical particle size, which was directly associated with the experimentally measured result as displayed in Fig. 3 of the next section. The permeate flux adopted a modified Hermia's semi-empirical expression of time dependent flux due to pore blocking,[20,35] as follows:

$$J(t) = J_0 e^{-\alpha t} + J_{b0}(1 - e^{-\alpha t}) \tag{12}$$

where J_0 and J_{b0} are the permeate fluxes for the clean and blocked supports, respectively, which were all determined by experiment. The blocking coefficient, α (s^{-1}), was derived according to the literature.[20]

$$\alpha = \frac{1.5c_s^2 J_0 d_r^4}{d_{crit}^5} \tag{13}$$

where d_r (m) is the average pore diameter of support, which was the experimental value as given in the next section.

The layer thickness growth rate, $h(t)$ (m s^{-1}), can be calculated using the following equation:[26]

$$h(t) = \frac{m(t)}{\rho_s[1 - \varepsilon(t)]} \tag{14}$$

where the dynamic layer porosity, $\varepsilon(t)$, was derived by combining Eq. (13) with the modified Ergun equation,[36] as follows:

$$\varepsilon(t) = 1 - \frac{\Delta P d_{crit}^2 \rho_s \varepsilon(t)^3}{150\mu J(t) m(t)} \tag{15}$$

where ΔP (Pa) is the trans-membrane pressure difference.

Therefore, the dynamic layer thickness, H_{DM} (m), can be determined as below:

$$H_{DM} = \int_0^t h(t)dt \tag{16}$$

Experimental

Figure 2 shows the experimental setup used for DM formation. Zirconium dioxide (ZrO_2) particles were selected as the coating material (analytical grade, Aladdin, China) with the density of 5850 kg m^{-3}. The particle size distribution of ZrO_2 was measured using a centrifugal particle size analyzer (SA-CP3, Shimadzu, Japan) at the State Key Laboratory of Fine Chemicals in Dalian University of Technology (DUT). The average particle size was obtained to be 2.05 μm. Fig. 3 shows the mass accumulation fraction, Q_m, of the ZrO_2 particles. Porous carbon tubes used as the supports were provided by the Membrane Science and Research Development Centre of

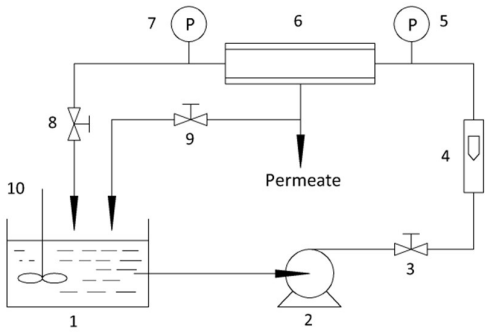

Fig. 2 Schematic diagram of the experimental setup. (1) Storage tank; (2) centrifugal pump; (3, 8 and 9) valves; (4) flowmeter; (5 and 7) pressure gauges; (6) membrane module; (10) stirrer.

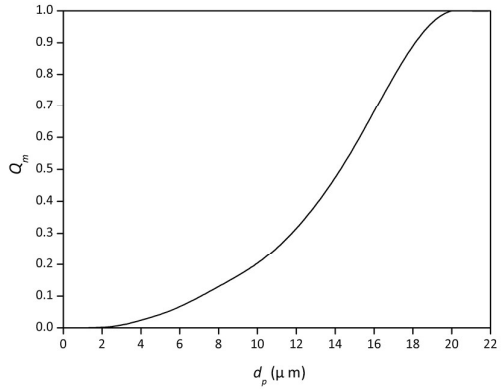

Fig.3 Mass accumulation fraction of ZrO_2 particles.

DUT. Characteristics were measured using the bubble-pressure method with isopropanol as the wetting liquid and nitrogen as the porometry gas at room temperature.[37] The average pore size and porosity were 1.7 μm and 41.22%, respectively. The tubes had 5 mm in inner diameter, 9mm in outer diameter and 100 mm in effective length. Microfiltration operations were conducted under 0.10 MPa of the trans-membrane pressure difference, 20˚C of the feed temperature, 0.5 g L^{-1} of the feed concentration, and 1.136 and 1.420 m s^{-1}, respectively, of the cross-flow velocities. Detailed experimental procedures have been described elsewhere.[3]

The morphologies of the prepared DMs were observed by a scanning electron microscopy (SEM, YKYK-2800, China). The thicknesses of the dynamic layers were measured by an energy-dispersive X-ray spectrometer (EDX, YKYK-2800, China).

Results and discussion

To examine the effects of operating conditions on three critical particle sizes, the permeate flux, *J*, was studied as the primary affecting factor under different cross-flow velocities and feed temperatures. The operating conditions employed in the present tests were 0.10 MPa of the trans-membrane pressure difference, 0.5 g L^{-1} of the feed concentration, 0.5–2.0 m s^{-1} of the cross-flow velocities and 20–40˚C of the feed temperatures. The values of 0.10 MPa and 0.5 g L^{-1} were used in consistence with subsequent experimental conditions. Because the feed concentration was quite low, the density and viscosity of water were used instead of those of the feed. Particles located at 0, 90 and 180˚ of the angles were chosen for analyses.

Equations (6), (8), (10) and (15) were solved by the Newton-Raphson method with absolute errors below 10^{-13} for the three critical particle sizes and below 10^{-7} for the dynamic layer porosity.

Variations of critical particle sizes, $d_{crit,R}$, $d_{crit,C}$ and $d_{crit,A}$

Figure 4 shows the effects of the cross-flow velocities on the critical particle size, $d_{crit,R}$, in the radial direction at 30°C of the feed temperature, 0.10 MPa of the trans-membrane pressure difference and 0.5 g L^{-1} of the feed concentration. As the permeate flux was increased, the $d_{crit,R}$ gradually increased. This can be explained by a larger permeate flux resulting in a larger resultant force in the depositional direction, causing the particles to deposit easily. The $d_{crit,R}$ at the bottom (0˚) of the horizontal tube was greater than those at the side (90˚) and top (180˚). This was because smaller angles, ϕ, lead to larger gravitational components, causing the particles to deposit more easily. With increased cross-flow velocities, the lateral lift force and shear-induced force increased, and the particles became difficult to deposit. At the small cross-flow velocity of 0.5 m s^{-1} in Fig. 4, a large difference between the critical particle sizes at different locations in different angles was observed. This indicated that a relatively small cross-flow velocity would not be beneficial to achieve uniformities of the $d_{crit,R}$ and dynamic layer during formation. As the cross-flow velocity was increased, this difference gradually was decreased and became negligible at 2.0 m s^{-1}. This suggested that an appropriately large cross-flow velocity between at 1.0 and 2.0 m s^{-1} was expected to prepare a desired DM with a uniform thickness. The case of 0.5 m s^{-1} can therefore be ignored.

Fig. 4 Variations of $d_{crit,R}$ with *J* at different cross-flow velocities.

Figure 5 shows the effects of the feed temperatures on $d_{crit,R}$ at 1.0 m s^{-1}, 0.10 MPa and 0.5 g L^{-1}. The $d_{crit,R}$ decreased as the temperature was increased, and $d_{crit,R}$ differences always existed at different intersection angles. Because the permeate flux increased as the temperature was increased, the normal drag force, F_y, positively affected the resultant force, as shown in Eq. (1). However, the Brownian diffusion force, F_c, had a negative effect on the resultant force as shown in Eq. (4). The lateral lift force in Eq. (2) and the shear-induced force in Eq. (3) remained unchanged. In addition to the gravitational component in the radial direction, only the normal drag force and Brownian diffusion force therefore contributed to the resultant force. The Brownian diffusion force may be more significant than the normal drag force, which was probably the reason why increasing the temperature was not favorable for particle deposition. Nevertheless, such an effect was relatively small compared with the effect of the cross-flow velocity and may be negligible.

Because 0.5 m s^{-1} of the cross-flow velocity was not a good operating condition as analyzed previously, it is not included in

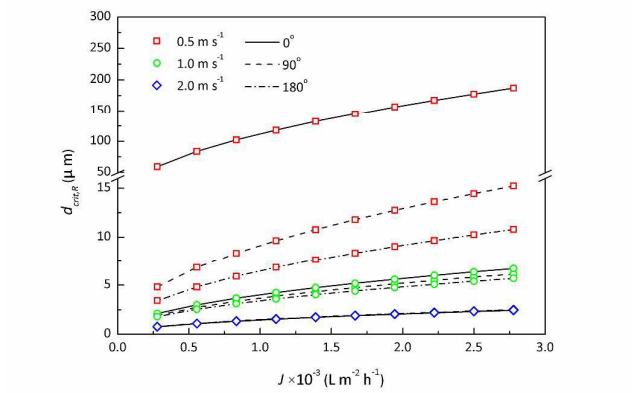

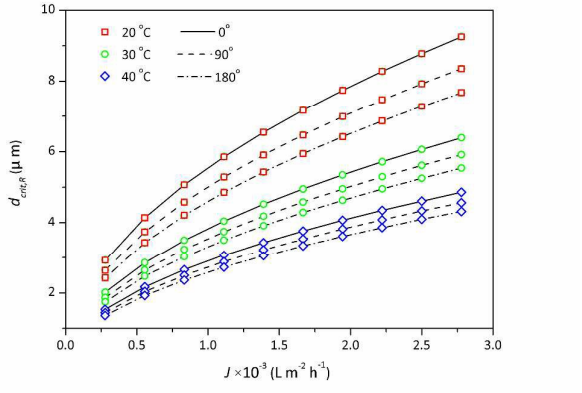

Fig. 5 Variations of $d_{crit,R}$ with J at different temperatures.

subsequent discussions. Fig. 6 shows variations of the critical particle size, $d_{crit,C}$, in the circumferential direction with J under 1.0 and 2.0 m s^{-1} of the cross-flow velocities at 30 °C, 0.10 MPa and 0.5 g L^{-1}. The permeate flux had little effect on the $d_{crit,C}$, and a larger cross-flow velocity was still helpful for uniformity of the $d_{crit,C}$. As the angle was increased, the gravitational component in the circumstantial direction would increase and the resultant force in the depositional direction would therefore decrease. This would possibly result in the particles to roll at a given cross-flow velocity. As the cross-flow velocity was increased, the radial resultant force would decrease, allowing the particles to roll more easily. Although different cross-flow velocities lead to different critical particle sizes, it should be carefully selected to prevent particles from rolling in the circumstantial direction.

Figure 7 shows the effects of the feed temperature on the $d_{crit,C}$ at 1.0 m s^{-1}, 0.10 MPa and 0.5 g L^{-1}. The flux still had little effect on the $d_{crit,C}$, as observed in Fig. 6 previously and the temperature had a effect on the $d_{crit,C}$ similar to the cross-flow velocity. Differences in the $d_{crit,C}$ at different locations did not obviously decrease as the temperature was increased. Although increasing the temperature resulted in a smaller critical particle size, the temperature effect on the $d_{crit,C}$ was far from significant compared with the cross-flow velocity.

Fig. 7 Variations of $d_{crit,C}$ with J at different feed temperatures.

Figure 8 shows variations of the axial critical particle size, $d_{crit,A}$, as a function of permeate flux at different cross-flow velocities at 30°C, 0.10 MPa and 0.5 g L^{-1}. The $d_{crit,A}$ was less sensitive to the flux. The effect of the cross-flow velocity on the $d_{crit,A}$ was similar to the effect on the $d_{crit,C}$ as shown in Fig. 6. However, the difference between the axial critical particle sizes at different angles has become less significant for a given cross-flow velocity. This suggested that the dynamic layer with a uniform thickness could be obtained if the $d_{crit,A}$ were the major concern. At a small cross-flow velocity, relatively large particles may roll on the dynamic layer surface due to a large axial component of the radial resultant force and a small cross-flow drag force along the axial direction. In contrast, at a large cross-flow velocity, relatively small particles may be unstable within the fluid.

Figure 9 shows variations of the axial critical particle size, $d_{crit,A}$ with permeate flux at different feed temperatures. The temperature had reverse effects on the $d_{crit,A}$, as shown in Fig. 9, in comparison with the $d_{crit,R}$ and $d_{crit,C}$, as observed previously. As the temperature was increased, the $d_{crit,A}$ slightly increased. This is due to small radial resultant forces at relatively high temperatures. As a result, the particle may roll along the axial direction under high temperature conditions. However, variations of the $d_{crit,A}$ caused by temperature

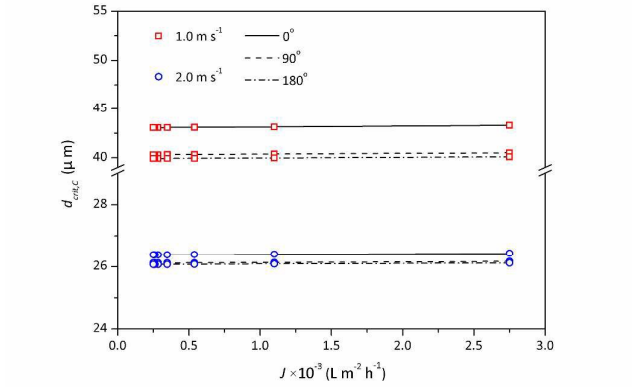

Fig. 6 Variations of $d_{crit,C}$ with J at different cross-flow velocities.

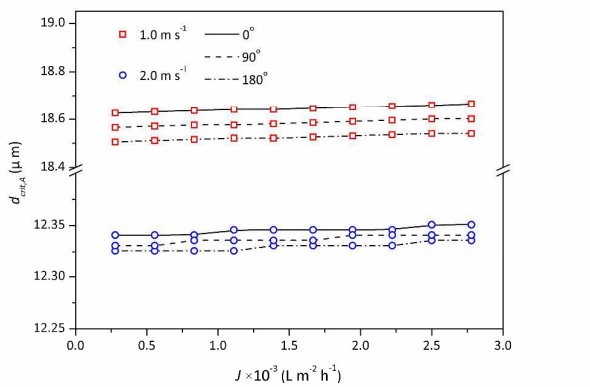

Fig. 8 Variations of $d_{crit,A}$ with J at different cross-flow velocities.

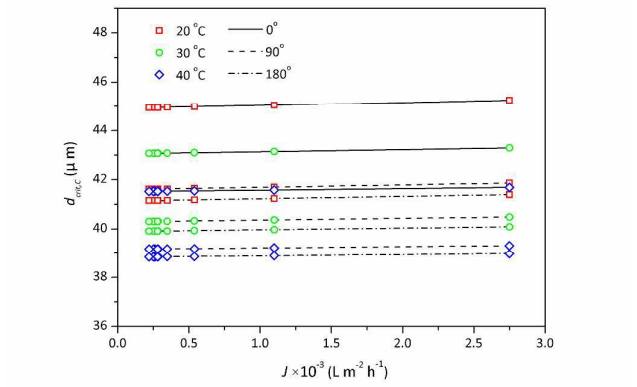

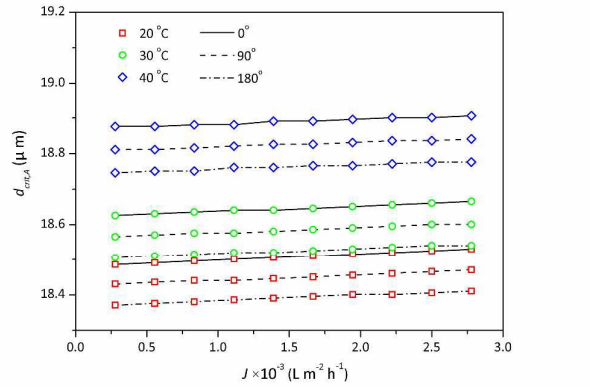

Fig. 9 Variations of $d_{crit,A}$ with J at different feed temperatures.

variations were so small that it was not worth considering compared with the $d_{crit,R}$ and $d_{crit,C}$.

Comprehensive analysis of particle deposition

In the present study, four steps were employed to determine whether or not a particle could be deposited onto the inner surface of a horizontal tubular support during cross-flow microfiltration, as listed below.

(1) If it is possible for a particle to deposit in the radial direction under exertion of the radial resultant force.

(2) If it is possible for a particle to roll along the circumferential direction under exertion of the circumferential moment.

(3) If it is possible for a particle to roll along the axial direction under exertion of the axial moment.

(4) If it is possible for a particle to implement real deposition by comparing three types of the critical particle sizes.

To match the experimental operating conditions, calculations were again conducted under typical operating conditions at 0.10 MPa, 20°C and 0.5 g L^{-1} at 1.420 m s^{-1} located at 0°, as shown in Fig. 10. Among the three critical sizes, the smallest size is the controlling one during the formation of a DM. It is impressive to observe that the circumferential critical particle size, $d_{crit,C}$, was always greater than the other two types throughout the flux variation range, which was not predominant. However, for the radial and axial critical particle sizes, which one was the controlling factor depended on the flux value that divided the overall operation into two regions. When the flux was less than 0.05 L m^{-2} h^{-1}, the radial critical particle size, $d_{crit,R}$, played a major role; while when the flux was higher than 0.05 L m^{-2} h^{-1}, the axial critical particle size, $d_{crit,A}$, controlled particle deposition. Under the present operating conditions (trans-membrane pressure difference of 0.10 MPa, cross-flow velocity ranging from 1.0 to 2.0 m s^{-1} and feed temperature below 40°C), the DM operating region for particle deposition was located within region I, which indicated that the $d_{crit,R}$ was the sole determinant.

Experimental observation of particle deposition

To verify the above simulation results, two DMs were prepared

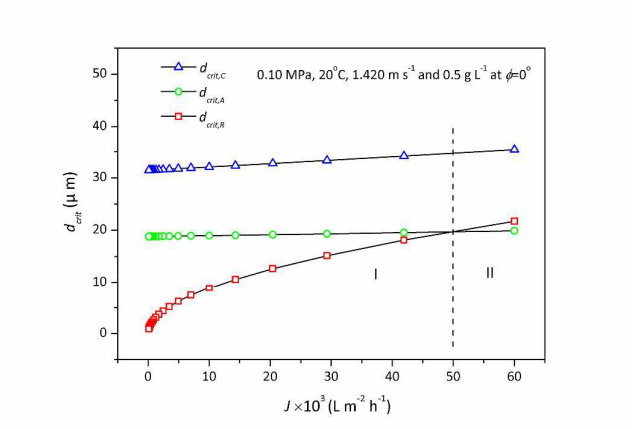

Fig. 10 Variations of $d_{crit,R}$, $d_{crit,C}$ and $d_{crit,A}$ with J.

under the cross-flow velocities of 1.136 and 1.420 m s^{-1}, respectively, under the typical operating conditions as stated in the last section. The prepared DMs were characterized with a scanning electronic microscope (SEM). The SEM allows direct observation of the surface features of a specimen due to its huge magnifications and impressive resolutions at the micron and submicron levels.

Fig. 11 shows the SEM images of cross sections of the prepared DMs. At a small cross-flow velocity, as shown in Figs. 11(a), (b) and (c), different layer thicknesses were observed at different angles. The dynamic layer was thicker at the bottom (0˚), thinner at the top (180˚) and in between at the side (90˚). More importantly, the particle sizes at the bottom were obviously larger than those at the top. This means that large particles easily deposited at the bottom under a relatively small cross-flow velocity, which was qualitatively consistent with the previous analyses. At a high cross-flow velocity, as shown in Figs. 11(d), (e) and (f), the layer became thin and the particle sizes looked uniform compared with the case of the small cross-flow velocity. This again demonstrated that an appropriately large cross-flow velocity was a beneficial operating condition for uniform thickness in DM preparation.

Comparison of predictions with experiments

Figure 12 shows the experimentally measured permeate flux data and flux curves predicted with Eq. (12). Good agreements implied that the equation can sufficiently reproduce variations of the permeate flux with time.

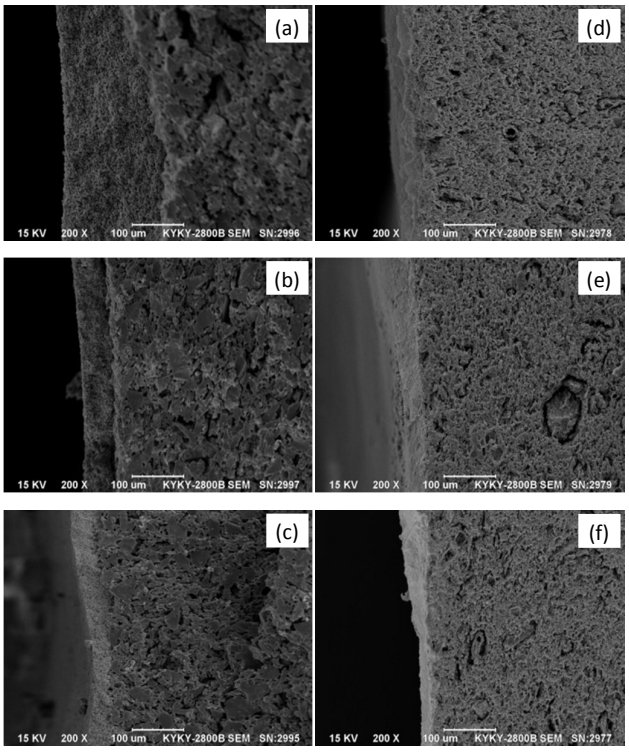

Fig. 11 SEM images of cross sections of ZrO_2 DM at different locations. (a) 0˚, (b) 90˚ and (c) 180˚ at 1.136 m s^{-1}; (d) 0˚, (e) 90˚ and (f) 180˚ at

1.420 m s^{-1}.

Figure 13 illustrates the three-dimensional diagram of dynamic layer thicknesses under different cross-flow velocities predicted with Eq. (16). As the intersection angle, ϕ, was increased, the thickness gradually became thinner. This non-uniform thickness distribution was due to the decrease in the critical size of the deposited particles as the angle was decreased, leading to decreased deposition quantity in the upper part of the circumference. Under a relatively large cross-flow velocity, the layer thickness was found to be thinner but more uniform, which is consistent with previous analyses.

Figures 14 and 15 show comparisons between the experimental data and predicted results of DM thicknesses. The calculated layer thicknesses impressively displayed excellent agreements with the experimental measurements. This demonstrates that the developed critical particle size models can accurately reproduce particle deposition and layer growth during DM preparation with cross-flow microfiltration. More significantly, specifically pre-designed dynamic layer structures can be generated by altering the operating parameters for various DM filtration purposes.

Effects of trans-membrane pressure difference and concentration

To further examine the effects of operating conditions on particle deposition and layer growth, predictions were also performed under different trans-membrane pressure differences and feed concentrations. These two parameters were selected because the temperature had a negligible effect on the process, as analyzed previously. Fig. 16 shows variations of the dynamic layer thickness under the trans-membrane pressure differences of 0.06, 0.10 and 0.14 MPa. The pressure difference had little influence on the layer uniformity. This was because the pressure difference had the same effect on the critical particle sizes and coating particle distributions along the circumferential direction. A large pressure difference resulted in a thin dynamic layer, as shown in Fig. 16. This was due to a decreased porosity of the layer under an increased pressure difference, causing a dense layer and a high resistance consequently. Therefore, the trans-membrane pressure difference should not be adopted as an adjusting parameter during DM formation.

Figure 17 shows variations of the dynamic layer thickness under the feed concentrations of 0.2, 0.5 and 0.8 g L^{-1}. As the concentration was increased, the layer thickness increased as expected. This would lead to a high resistance. Careful observation of Fig. 17 also found that larger concentrations resulted in a layer with less uniformity. This suggested that a larger concentration was not a good operating condition

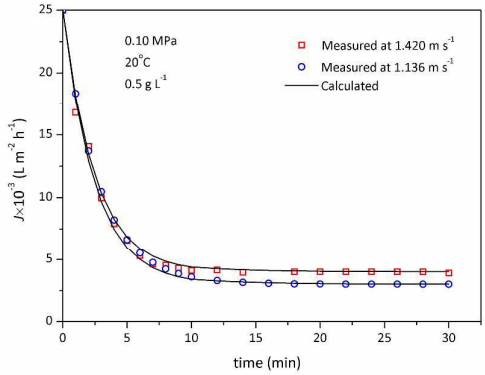

Fig. 12 Comparisons of calculated with measured permeate fluxes.

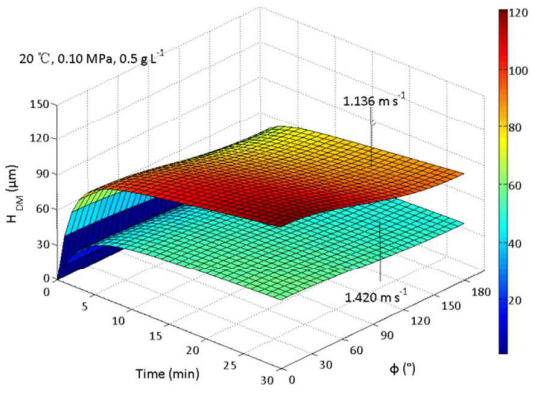

Fig. 13 Variations of layer thickness at different cross-flow velocities

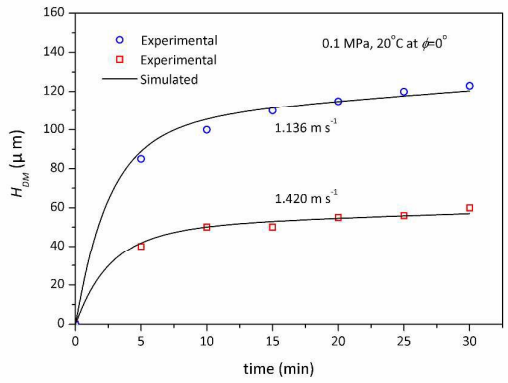

Fig. 14 Comparisons of predicted and measured thickness with time.

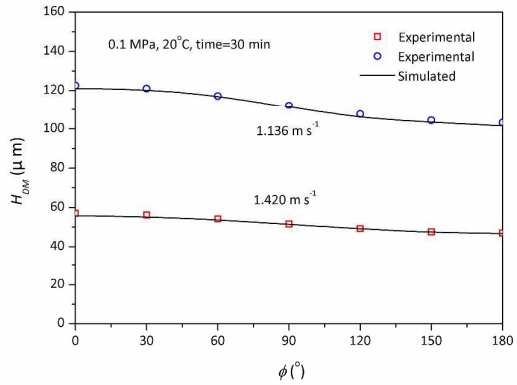

Fig. 15 Comparisons of predicted and measured thickness with angle.

although it can be used to adjust the layer thickness.

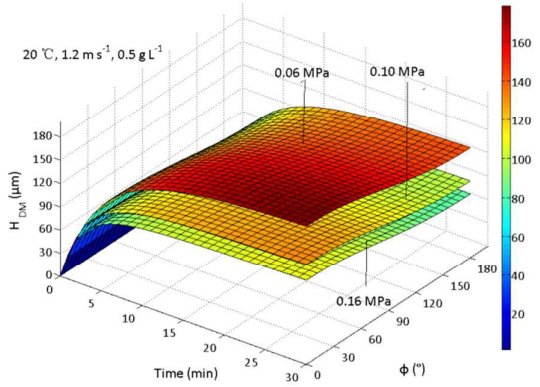

Fig. 16 Variations of thickness with different pressure differences.

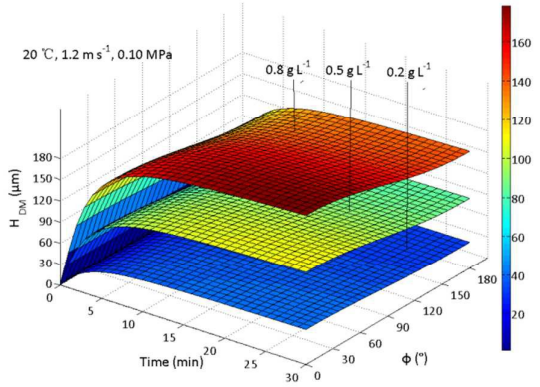

Fig. 17 Variations of thickness with different feed concentrations.

In a word, quantitative prediction of particle deposition and layer growth in preparing a pre-coated DM is feasible and effective as studied in the present work. Among the four operating conditions, i.e., cross-flow velocity, feed temperature, trans-membrane pressure difference and feed concentration, the cross-flow velocity can be used as the controlling parameter to achieve a thin and uniform dynamic layer with a certain thickness. An appropriately large cross-flow velocity with a small pressure difference and a low concentration was beneficial to prepare a desired DM. The temperature effect can be negligible.

Conclusion

Theoretical and experimental investigations were conducted in the present work aimed at predicting particle deposition and layer growth during preparation of a dynamic membrane with cross-flow microfiltration. The simulation results showed that the critical particle size decreased as the cross-flow velocities and/or the feed temperatures were increased. The influence of the feed temperature can be ignored compared with the cross-flow velocity. The critical particle size in the radial direction was the controlling factor among the three types for particle deposition during DM formation under the tested operating conditions. Both the predicted and experimental results showed that the deposited particles were not uniformly distributed along the circumferential direction within the horizontal tube, and the dynamic layer at the bottom of the tube was thicker than those at the side and top due to the gravitational effect. The cross-flow velocity was a good operating parameter in controlling the dynamic layer thickness and uniformity. As the cross-flow velocity was appropriately increased, the layer became thinner and more uniform. Comparisons of the model predictions with experimental data of DM thicknesses displayed good agreements, indicating that the developed critical particle size model can accurately preidct particle deposition and layer growth during DM formation with cross-flow microfiltration. The simulation also showed that the increased trans-membrane pressure difference lead to a thin and dense layer, but had no effect on the layer uniformity. A relatively low feed concentration resulted in a thinner and more uniform layer.

Acknowledgements

The authors greatly appreciate the financial supports from the National Natural Science Foundation of China (NSFC20976020) and the Fundamental Research funds for the Central Universities of China (DUT13JN04).

Notes and references

1 A. E. Marcinkowsky, K. A. Kraus, H. O. Phillips, J. S. Johnson Jr. and A. J. Shor, *J. Am. Chem. Soc.*, 1966, **88**, 5744.
2 S. Kishihara, H. Tamaki, S. Fujii, and M. Komoto, *J. Membr. Sci.*, 1989, **41**, 103.
3 Y. Q. Pan, T. T. Wang, H. M. Sun and W. Wang, *Sep. Purif. Technol.*, 2012, **89**, 78.
4 C. C. Chen and B. H. Chang, *J. Membr. Sci.*, 1998, **143**, 65.
5 J. Y. Wang, M. C. Liu and C. J. Lee, *J. Membr. Sci.*, 1999, **144**, 45.
6 M. Marcucci, G. Nosenzo, G. Capannelli, I. Ciabatti, D. Corrieri and G. Ciardelli, *Desalination*, 2001, **138**, 75.
7 M. J. M. M. Noor, F. R. Ahmadun, T. A. Mohamed, S. A. Muyibi and M. B. Pescod, *Desalination*, 2002, **147**, 263.
8 Y. J. Zhao, Y. Tan, F. S. Wong, A. G. Fane and N. P. Xu, *Sep. Purif. Technol.*, 2005, **44**, 212.
9 T. V. Knyazkova and A. A. Kavitskaya, *Desalination*, 2000, **131**, 129.
10 V. T. Kuberkar and R. H. Davis, *J. Membr. Sci.*, 2000, **68**, 243.
11 M. T. P. de Amorim and I. R. A. Ramos, *Desalination*, 2006, **192**, 63.
12 T. Yang, Z. F. Ma and Q. Y. Yang, *Desalination*, 2003, **270**, 50.
13 A. E. Marcinko, K. A. Kraus, H. O. Phillips, J. S. Johnson and A. J. Shor, *J. Am. Chem. Soc.*, 1966, **88**, 5744.
14 G. B. Tanny, *Sep. Purif. Methods*, 1978, 7, 183.
15 M. H. AlMalack and G. K. Anderson, *J. Membr. Sci.*, 1996, **112**, 287.
16 M. -C. Vincent-Vela, B. Cuartas-Uribe, S. Alvarez-Bianco and J. Lora-Garcia, *Chem. Eng. Process.*, 2011, **50**, 404.
17 V. L. Pillay, Modeling of the turbulent cross-flow microfiltration of particles suspensions, PhD thesis, University of Natal, Durban, South Africa, 1997.

18 R. H. Davis and D. T. Leighton, *Chem. Eng. Commun.*, 1987, **42**, 275.
19 C. A. Romero and R. H. Davis, *J. Membr. Sci.*, 1988, **39**, 157.
20 L. F. Song, *J. Membr. Sci.*, 1998, **139**, 183.
21 L. Y. Wang and L. F. Song, *J. Membr. Sci.*, 1999, **160**, 41.
22 G. Schulz and S. Ripperger, *J. Membr. Sci.*, 1987, **40**, 173.
23 J. W. Hunt, K. Treffrygoatley, R. L. C. Flemmer, J. D. Raal and C. A. Buckley, *Desalination*, 1987, **61**, 187.
24 T. W. Perkins, S. Saksena and R. van Reis, *J. Membr. Sci.*, 1999, **158**, 243.
25 N. J. Blake, I. W. Cumming and M. Streat, *J. Membr. Sci.*, 1992, **68**, 205.
26 J. Altmann and S. Ripperger, *J. Membr. Sci.*, 1997, **124**, 119.
27 D. J. Chang, F. C. Hsu and S. J. Hwang, *J. Membr. Sci.*, 1995, **98**, 97.
28 Z .Q. Wang, *Applied Mathematics and Mechanics*, 1982, **3**, 443.
29 M. R. Wiesner, M, M. Clark and J. Mallevialle, *J. Environ. Eng.*, 1989, **115**, 20.
30 R. D. Cohen and R. F. Probstein, *J. Colloid Interface Sci.*, 1986, **114**, 194.
31 D. A. Drew, J. A. Schonberg and G. Belfort, *Chem. Eng. Sci.*, 1991, **46**, 3219.
32 H. C. Hamaker, *Physica*, 1937, **4**, 1058.
33 A. Vantent and K. Tenijenhuis, *J. Colloid Interface Sci.*, 1992, **150**, 97.
34 R. M. McDonogh, C. J. D. Fell and A. G. Fane, *J. Membr. Sci.*, 1984, **21**, 285.
35 J. Hermia, *Trans. Inst. Chem. Eng.*, 1982, **60**, 183.
36 Y. K. Benkahla, A. Ould-Dris, M. Y. Jaffrin and D. Si-Hassen, *J. Membr. Sci.*, 1995, **98**, 107.
37 Y. Q. Pan, W. Wang, T. H. Wang and P. J. Yao, *Sep. Purif. Technol.*, 2007, **57**, 388.